

Reexamination of Damping in Sliding Friction

Shuyu Huang^{1,3,*}, Zhiyong Wei^{1,*}, Zaoqi Duan^{1,*}, Chengdong Sun^{1,*}, Yongkang Wang,¹ Yi Tao¹, Yan Zhang,¹ Yajing Kan¹, Ernst Meyer³, Deyu Li^{2,†} and Yunfei Chen^{1,‡}

¹*Jiangsu Key Laboratory for Design and Manufacture of Micro-Nano Biomedical Instruments, School of Mechanical Engineering, Southeast University, Nanjing 211189, China*

²*Department of Mechanical Engineering, Vanderbilt University, Nashville, Tennessee 37235-1592, USA*

³*Department of Physics, University of Basel, Basel, Switzerland*



(Received 8 January 2023; accepted 12 December 2023; published 30 January 2024)

Friction is responsible for about one-third of the primary energy consumption in the world. So far, a thorough atomistic understanding of the frictional energy dissipation mechanisms is still lacking. The Amontons' law states that kinetic friction is independent of the sliding velocity while the Prandtl-Tomlinson model suggests that damping is proportional to the relative sliding velocity between two contacting objects. Through careful analysis of the energy dissipation process in atomic force microscopy measurements, here we propose that damping force is proportional to the tip oscillation speed induced by friction. It is shown that a physically well-founded damping term can better reproduce the multiple peaks in the velocity-dependent friction force observed in both experiments and molecular dynamics simulations. Importantly, the analysis gives a clear physical picture of the dynamics of energy dissipation in different friction phases, which provides insight into long-standing puzzles in sliding friction, such as velocity weakening and spring-stiffness-dependent friction.

DOI: [10.1103/PhysRevLett.132.056203](https://doi.org/10.1103/PhysRevLett.132.056203)

Even in rudimentary physics textbooks, the phenomenological Amontons-Coulomb friction law, $F_f = \mu_k N$, is often included, stating that kinetic friction force (F_f) is equal to a kinetic friction coefficient (μ_k) times the normal load (N) and is independent of contact area and relative sliding velocity [1–3]. However, until now it is still impossible to derive this friction law from first principles and a thorough understanding of the detailed dynamics of energy dissipation at the atomic scale is still lacking. In fact, efforts with modern instruments, such as the surface force apparatus [4–6], atomic force microscope (AFM) [7–11], and quartz crystal microbalance [12], have observed a sliding-velocity-dependent friction force that is obviously inconsistent with the Amontons-Coulomb law. Meanwhile, atomistic models, including the classical Prandtl-Tomlinson (PT) [13,14] and Frenkel-Kontorova (FK) [15–17] models and various modifications [9,18], have been used to explain the velocity dependence in sliding friction. While these models have been able to explain some experimental trends, they cannot account for other important observations. So far, there is no theoretical model that can predict kinetic friction force over a wide sliding velocity range.

In an ultralow sliding velocity regime below several hundred nm/s, the PT model can well reproduce the velocity-independent stick-slip events observed in AFM experiments [7,8,18]. However, the PT model prediction quickly deviates from the experimental observation as the sliding velocity increases to several $\mu\text{m/s}$, and modifications to the model have to be introduced to account for

experimental observations. For instance, to resolve the velocity-dependent friction, a thermally activated PT model [9] was proposed to explain the logarithmic experimental trend [19], which is attributed to thermally actuated transitions between neighboring potential wells [20–23]. Still, phenomena such as velocity weakening [24–26], and especially nonmonotonic variations [27] in the mean friction force, pose challenges to the theoretical understanding. The large number of experimental results deviating from the PT model indicate that the damping term might not correctly reflect the energy dissipation in sliding friction. Here, through systematic AFM measurements over a wide range of sliding velocity under different normal loads, we propose that damping force is proportional to the tip oscillation speed, which better reflects the kinetic energy dissipated by phonons and recaptures both experimental and molecular dynamics (MD) results.

We measure the friction force as a silicon tip slides over a piece of molybdenum disulfide (MoS_2) flake along the zigzag direction as shown schematically in Fig. 1(a). All measurements are carried out in the ambient conditions with a temperature of $\sim 25^\circ\text{C}$ and a relative humidity of $\sim 25\%$ (See experimental details in the Supplemental Material [28]). Figure 1(c) plots the measured mean friction force versus the substrate sliding velocity in the range from 8.14 to 122.07 $\mu\text{m/s}$ under three different normal loads of 10, 30, and 60 nN, respectively. The mean friction force displays an increasing trend with the load but exhibits a nonmonotonic profile with the sliding velocity. As the sliding velocity

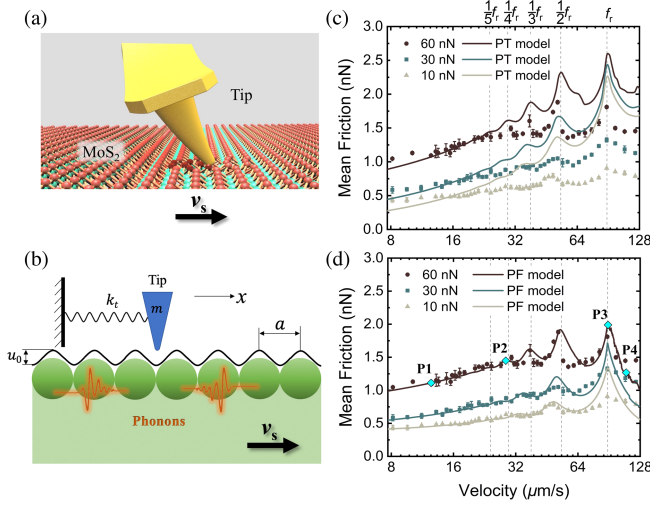


FIG. 1. Schematic illustration of (a) an AFM used to measure friction force as its tip slides over a MoS₂ substrate. (b) A simplified friction model for the friction force measurement with an AFM, which describes the energy dissipation process in sliding friction. (c) The measured friction force (dots) and the best fitting with the classical PT model (solid lines). (d) The measured friction force and the fitting with the proposed phononic friction (PF) model. The scan size in the experiments is $5 \times 5 \mu\text{m}^2$. The periodic length along the sliding direction is determined to be $a = 0.316 \text{ nm}$. Note that f_r in (c) and (d) stands for the torsional resonant frequency (f_r) of the cantilever, which depends on the sliding velocity because the contact stiffness varies with the sliding velocity. This implies that the tip-substrate system at each sliding velocity has a specific resonant frequency f_r .

increases beyond $\sim 25 \mu\text{m/s}$, several peaks in the mean friction force can be clearly identified, similar to what we recently reported for the study with a graphite substrate [27].

To understand the atomistic mechanisms that lead to the observed friction force, we first try to fit the experimental data using the classical PT model. As shown in Fig. 1(b), the PT model describes an AFM tip attached to an anchor through a spring sliding over a substrate that is represented by a sinusoidal potential. If we assume that the anchor is stationary and the original point is taken as the location of the tip under relaxed condition and the substrate is moving with a constant velocity v_s along the x direction, the one-dimensional PT model can be written as

$$m\ddot{x} + m\mu(\dot{x} - v_s) + k_t x = -\frac{\partial U(x, t)}{\partial x}. \quad (1)$$

Here x is the tip displacement. m and k_t are the mass and the spring constant, which correspond to the effective mass of the tip and the torsional spring constant for the cantilever along the sliding direction in the AFM setup, respectively. k_t and m can be determined by experiments (see Secs. 4 and 8 of the Supplemental Material [28]). μ is the damping coefficient describing the frictional energy dissipation, and U is the corrugated surface potential given by

$$U(x, t) = -\frac{u_0}{2} \cos \left[2\pi \left(\frac{x - v_s t}{a} \right) \right], \quad (2)$$

where a and $(u_0/2)$ are the period length and amplitude of the corrugated potential, respectively. u_0 is related to the normal load and can be fitted from the corresponding experimental results, which yields 1.02, 1.38, and 1.98 eV for the normal load of 10, 30, and 60 nN, respectively. The damping coefficient μ is related to the damping ratio (β) defined as $\beta = (\mu/\mu_c)$, where μ_c is the critical damping coefficient of the system calculated by $\mu_c = 2\sqrt{(k_t/m)}$. The instantaneous friction force can be reflected by the spring force, $F_f = -k_t x$. A damping ratio of 0.14 yields the best fitting for all three normal load cases, which suggests that the setup with a tip sliding over the MoS₂ substrate corresponds to an underdamping system [35].

Based on these parameters, a fourth-order Runge-Kutta algorithm is used to solve the PT model [36], and the results are shown in Fig. 1(c). The PT model yields an increasing friction force in the velocity range of 8 to 25 $\mu\text{m/s}$, which is consistent with the experimental results; however, the escalation slopes for all three normal loads are larger than those of the experimental results. The deviation from the experimental data becomes more unacceptable as the sliding velocity increases beyond 25 $\mu\text{m/s}$. To further understand why the PT model fails to recapture the experimental results, we examine the damping term in Eq. (1), which is proportional to the relative sliding velocity between the tip and substrate, and the corresponding dissipated energy, E_d^{PT} , can be expressed as

$$E_d^{PT} = \int_0^t m\mu(\dot{x} - v_s) \cdot (\dot{x} - v_s) dt. \quad (3)$$

The damping force of $m\mu(\dot{x} - v_s)$ is a linear-response type dissipative force, which is only valid at low sliding velocity [27,37]. The second term $(\dot{x} - v_s)dt$ stands for the relative displacement between the substrate and tip over a differential time dt . Equation (3) implies that there exists a dissipative force on the interface between the elastic tip and substrate to dissipate the kinetic energy of relative motion. Our MD simulation model demonstrates that the in-plane component of the combined force over the entire interfacial molecule-molecule interactions describes exactly the friction force, which indicates that only intermolecular force exists between two contacting elastic objects under a normal load (Sec. 1 in the Supplemental Material [28]). It should be noticed that the intermolecular force is only responsible for the conversion between the kinetic and potential energy. Contrary to the assumption in the classical PT model, there is no dissipative force presenting at the interface between two contacting objects to dissipate their kinetic energy. Instead, the energy dissipation happens in the bulk, which is mediated by the material internal degrees of freedom in the two contacting elastic objects.

We simplify the cantilever tip in an AFM as a spring-damper sphere, the substrate can be treated as an infinite substrate. Carefully analyzing the dynamic response of the sphere sliding over the substrate, we find that energy barriers are formed along the sliding direction due to the intermolecular interactions among the numerous interfacial molecules. It is the intermolecular force that resists the relative motion and deforms the elastic substrate and cantilever to accumulate potential energy. Once the potential energy is accumulated high enough to overcome the energy barrier, the slip phase starts. In the slip process, part of the accumulated elastic energy in the infinite substrate is released as elastic waves transporting away as phonons that never come back. For the spring-damper sphere, the released potential energy is converted to the sphere kinetic energy and dissipated by the cantilever internal damping. The total dissipated energy can be expressed as

$$E_d = \int_0^t m\mu_t \dot{x}^2 dt + \int_0^t \sum_{i=1}^n M\mu_i (\dot{x}_i - v_s)^2 dt, \quad (4)$$

where t stands for time, μ_t stands for the effective cantilever internal damping coefficient, μ_i and \dot{x}_i stands for the damping coefficient and instantaneous velocity of the atom i as shown in Fig. S4 in the Supplemental Material [28]. The first term stands for that the energy is dissipated by the cantilever tip due to the material internal damping. The second term stands for the released potential energy in the substrate as phonons.

As shown in Fig. 1(b), the interaction between the atoms of the sphere and the substrate is accurately captured using the Lennard-Jones (LJ) potential. To approximate the overall interaction that encompasses the entire sphere and substrate, a sinusoidal potential can be employed, which is derived by summing all atom-atom interactions, as shown in Eq. (2). In the whole stick-slip process, the interaction between the sphere and substrate is responsible only for the conversion between the potential and kinetic energy. As discussed in the Sec. 2 of the Supplemental Material [28], the released potential energy in the spring-damper sphere is proportional to the released potential energy in the substrate. We can employ an effective material internal damping coefficient, μ , to characterize the energy dissipation by the internal degrees of freedom within the friction system.

$$E_d = \int_0^t m\mu \dot{x}^2 dt = \int_0^t m\mu_t \dot{x}^2 dt + \int_0^t \sum_{i=1}^n M\mu_i (\dot{x}_i - v_s)^2 dt. \quad (5)$$

Here μ stands for an effective damping coefficient to describe the energy dissipated by the material internal damping in a friction system composed of two elastic objects such as the tip and substrate in Fig. 1. More details

about the formula derivation can be found in the Sec. 2 of the Supplemental Material [28]. \dot{x} is the tip oscillation speed relative to its equilibrium position. In this way, the damping coefficient μ has a clear physical meaning as that the energy is dissipated by oscillations, i.e., phonons. Integrating Eq. (5) with Newton's second law, a phononic friction model is proposed to describe the tip dynamical response induced by the relative motion,

$$m\ddot{x} + m\mu\dot{x} + k_t x = -\frac{\partial U(x, t)}{\partial x}. \quad (6)$$

In Eq. (6), the fundamental concept about frictional energy dissipation has been altered from that in the PT model as described by Eq. (1). The PT model suggests that the relative motion directly determines how much energy is dissipated as the damping force is directly proportional to the relative velocity between the tip and substrate. In contrast, Eq. (6) proposes that damping can only dissipate the energy acquired by the tip from the relative motion, which is more physically well founded because it precisely reflects that the energy is dissipated as elastic waves, i.e., the phonons. If no energy is acquired by the tip, no energy can be dissipated. The predicted results based on this phononic friction model are shown in Fig. 1(d), which fit the experimental data very well in the entire velocity range from 8 to 122 $\mu\text{m/s}$, and also recapture the frictional resonances to a much better level than the PT model. This strongly suggests that the proposed phononic friction model better reflects the actual energy dissipation process. We can also use the phononic friction model to fit MD simulation results, in which both the force magnitude and peak positions can be well predicted (more details can be found in Sec. 1 of the Supplemental Material [28]).

In the low-sliding-velocity range, the transient friction force can be obtained by the AFM as shown in Fig. S10 [28]. However, with the increase of sliding velocity, the low sampling frequency and inevitable noise in the AFM obscure the dynamics evolution of the friction force with time, which makes it difficult to understand the variations of the measured friction force in Fig. 1(d). With the help of Eq. (6), we can explain why the time-averaged friction force displays the nonmonotonic variation with sliding velocity, which is also frequently observed in the literature [24,27,38–42]. As displayed in Fig. 1(d), with the increase of the sliding velocity, the mean friction force displays (i) a monotonic increase trend ($<32 \mu\text{m/s}$), (ii) multiple oscillations with several peaks in the velocity range of $32 \mu\text{m/s} < v_s < 89 \mu\text{m/s}$, and (iii) a decreasing trend for $v_s > 89 \mu\text{m/s}$. At a low sliding velocity, such as $v_s = 12 \mu\text{m/s}$, the instantaneous friction force calculated from Eq. (6) exhibits a typical periodic stick-slip behavior with the same period length as that of the substrate potential [Fig. 2(a)]. Interestingly, the instantaneous friction force displays ringing oscillations after each slip event as shown in the

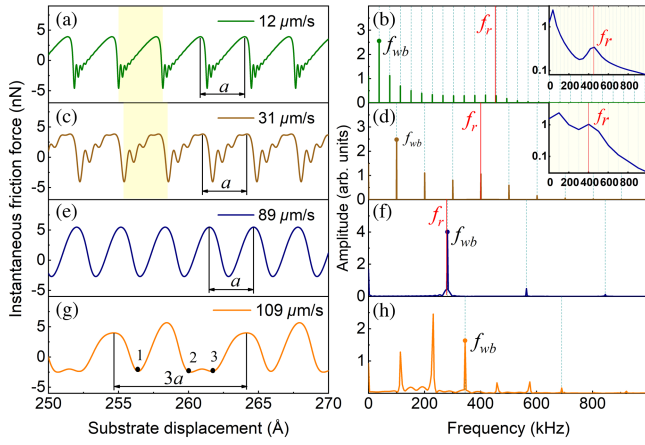


FIG. 2. The instantaneous friction force calculated from the phononic friction model [Eq. (6)] and its corresponding FFT spectrum at four representative sliding velocities: (a), (b) $v_s = 12 \mu\text{m/s}$, (c),(d) $v_s = 31 \mu\text{m/s}$, (e),(f) $v_s = 89 \mu\text{m/s}$, (g),(h) $v_s = 109 \mu\text{m/s}$. The insets in the right panel [(b) and (d)] stand for the FFT spectrum of the ringing oscillation. In the FFT figure, the green dotted lines represent the washboard frequency f_{wb} and nf_{wb} ($n = 1, 2, 3, \dots$) at the corresponding velocity.

highlighted yellow region in Fig. 2(a). Although the ringing oscillations are frequently observed in previous studies, their implications to energy dissipation have been rarely discussed [43–47]. As such, we conducted fast Fourier transform (FFT) analysis of the ringing oscillations, as shown in the inset of Fig. 2(b). The FFT spectrum clearly indicates a peak at the resonant frequency of the tip, f_r , which depends on the cantilever spring stiffness (k_t) and the tip-substrate contact stiffness (k_u), and can be expressed as [48]

$$f_r = \frac{1}{2\pi} \sqrt{\frac{k_{\text{eff}}}{m}} = \frac{1}{2\pi} \sqrt{\frac{k_t + k_u}{m}}. \quad (7)$$

Here k_u can be taken as the second derivative of the substrate corrugated potential with respect to the tip position. In fact, k_u is not a constant, which strongly depends on the sliding velocity and the tip position on the substrate potential. More details about the value of k_u at each velocity is discussed in the Sec. 11 of the Supplemental Material [28].

These ringing oscillations induce energy dissipation in addition to the asymmetric stick-slip events and are responsible to the fact that no friction force peak appears at low sliding velocities. As shown in Fig. 2(b), the FFT of the instantaneous friction force shows multiple peaks at the washboard frequency ($f_{wb} = v_s/a$) and its harmonics (nf_{wb}), which indicates that significant contributions to the friction force come from excess phonons excited at not only f_{wb} but also its harmonics, as discussed in Ref. [27]. What is missing in Ref. [27] is why no friction peak appears at relatively low sliding velocities, even when certain harmonic frequency of f_{wb} overlaps with the resonant

frequency. The ringing oscillations provide an explanation for this. For example, at the sliding velocity at $12 \mu\text{m/s}$, the corresponding f_{wb} is 37.97 kHz , far smaller than f_r which is 450.38 kHz . In this case, the tip has enough time to dissipate the residual energy through the ringing oscillations in the stick phase before it engages in the next slip event. As such, in the regime of $v_s < 25 \mu\text{m/s}$, the ringing oscillations are not able to overlap with the next slip event; and therefore resonant vibration cannot occur even when certain harmonic frequency of f_{wb} is equal to the resonant frequency.

As the sliding velocity increases, the oscillations persist over the entire period. In this case, if f_{wb} or its harmonics overlaps with the tip resonant frequency, i.e., $f_r = nf_{wb}$, resonance occurs and the friction force experiences a local peak. For example, when the sliding velocity is $31 \mu\text{m/s}$, $f_r \approx 4f_{wb}$ [as shown in Figs. 2(c) and 2(d) with $f_{wb} = 98.10$ and $f_r = 400.26 \text{ kHz}$], and the tip engages in resonant vibrations, leading to a local peak in the friction force as indicated by P2 in Fig. 1(d). In particular, for $v_s = 89 \mu\text{m/s}$ [corresponding to P3 in Fig. 1(d)], $f_r = f_{wb} = 281.89 \text{ kHz}$ [Figs. 2(e) and 2(f)], the excitation frequency is the same as the tip resonant frequency, which gives rise to the maximum friction force in the entire measurement velocity range. Once the sliding velocity v_s exceeds $89 \mu\text{m/s}$, $f_{wb} > f_r$, the dynamics of the tip becomes more complex because the fast excitation rate from the substrate potential is beyond the intrinsic rhythm of energy accumulation and dissipation in the tip-spring system. In this case, for example, at P4 with a sliding velocity of $109 \mu\text{m/s}$ [as shown in Figs. 2(g) and 2(h)], the periodic length for the instantaneous friction force is $3a$. Under this condition, during some stick-slip events, the substrate imparts more potential energy to the spring while during other events the substrate transfers little energy to the tip, which is evidenced by the low friction force between points 2 and 3 in Fig. 2(g). Notably, the $3a$ period does not qualify such event as a triple slip, but only indicates that $3a$ is required to constitute a complete cycle of energy accumulation and release.

It has been widely believed that the slip phase makes dominant contribution to energy dissipation in a stick-slip friction cycle [2]. Based on the variations of the spring force, a complete stick-slip cycle can be divided into three phases: stick, slip, and ringing oscillation (more detailed discussions can be found in Secs. 13 and 14 in the Supplemental Material [28]). The dissipated energy in each phase can be calculated by integrating the friction power dissipation over time, as shown in Fig. 3 with gray, green, and orange dots representing the dissipated energy in slip, oscillation, and stick phases, respectively. This dissipated energy for each sliding velocity is calculated over the substrate sliding distance of three lattice constants. At low sliding velocities (e.g., $12 \mu\text{m/s}$), the stick, oscillation, and slip phases contribute about 1%, 38%, and 61% to the

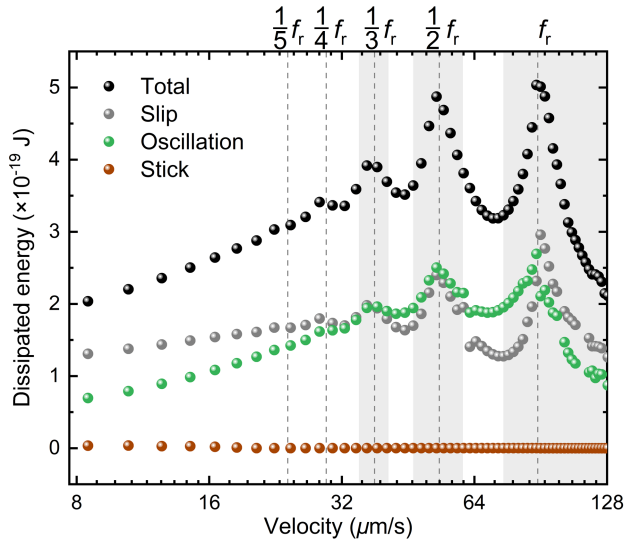


FIG. 3. Energy dissipation in the slip (gray dots), oscillation (green dots), and stick (orange dots) phases at various sliding velocities. Total dissipated energy is also presented with black dots for indication.

total dissipated energy, respectively, as shown in Fig. 3. As the sliding velocity rises, the energy dissipation due to oscillations increases and becomes comparable to that occurring during the slip phase. Particularly, when the tip engages in resonant vibrations, more kinetic energy is dissipated into heat, which leads to friction force peaks in Fig. 1(d).

In summary, we propose that the damping force is proportional to the tip oscillation speed in the AFM setup, which produces accurate predictions of the friction force obtained by AFM and MD results over a wide sliding velocity range. Given that the PT and FK models all have the same expression for the damping term and they have been used extensively to account for various friction phenomena, this new damping term could have immense implications to our understanding of the dynamics of energy dissipation at atomic scale. For example, existing models cannot quantitatively explain velocity weakening and other intriguing phenomena in experimental findings and engineering applications. In contrast, based on the proposed energy dissipation mechanism, we can account for spring-stiffness-dependent friction force and velocity weakening because the AFM cantilever spring stiffness directly determines the resonant frequency of the tip-substrate system. When resonance occurs, more energy is dissipated, which leads to enhanced friction force, i.e., multiple peaks in velocity-dependent friction. Once the sliding velocity exceeds the value corresponding to the condition of $f_r = f_{wb}$, the tip vibration cannot catch up with the periodic excitation of the substrate potential. In this case, the spring-mass system with a low resonant frequency cannot effectively acquire and dissipate energy from the moving substrate, which leads to a rapidly

decreasing friction force at even higher sliding velocity. Overall, the proposed phononic friction model provides an accurate tool to predict friction under different circumstances, which makes it possible to actively control friction in various applications.

The authors thank the Natural Science Foundation of China (Grants No. 52035003, No. 52127811, No. 51575104, No. 51705074, No. 52175161, and 2022ZB102). Z. W. acknowledges the Southeast University “Zhongying Young Scholars” Project. Y. C. also acknowledges the valuable inputs about energy dissipation process from Panyu Chen. E. M. acknowledges financial support from the Swiss National Science Foundation (SNF), the Swiss Nanoscience Institute (SNI) and the European Research Council (ERC) under the European Union’s Horizon 2020 research and innovation programme (ULTRADISS Grant Agreement No. 834402).

*These authors contributed equally to this work.

†Corresponding author: deyu.li@vanderbilt.edu

‡Corresponding author: yunfeichen@seu.edu.cn

- [1] J. Krim, Friction at the atomic scale, *Sci. Am.* **275**, No. 4, 74 (1996).
- [2] F. P. Bowden and D. Tabor, *The Friction and Lubrication of Solids* (Oxford University Press, Oxford, 2001).
- [3] D. Tabor, History of tribology: D. Dowson, *Tribol. Int.* **12**, 146 (1979).
- [4] M. Urbakh, J. Klafter, D. Gourdon, and J. Israelachvili, The nonlinear nature of friction, *Nature (London)* **430**, 525 (2004).
- [5] C. Drummond and J. Israelachvili, Dynamic phase transitions in confined lubricant fluids under shear, *Phys. Rev. E* **63**, 041506 (2001).
- [6] P. A. Thompson and M. O. Robbins, Origin of stick-slip motion in boundary lubrication, *Science* **250**, 792 (1990).
- [7] C. M. Mate, G. M. McClelland, R. Erlandsson, and S. Chiang, Atomic-scale friction of a tungsten tip on a graphite surface, *Phys. Rev. Lett.* **59**, 1942 (1987).
- [8] O. Zwörner, H. Hölscher, U. D. Schwarz, and R. Wiesendanger, The velocity dependence of frictional forces in point-contact friction, *Appl. Phys. A* **66**, S263 (1998).
- [9] E. Gnecco, R. Bennewitz, T. Gyalog, Ch. Loppacher, M. Bammerlin, E. Meyer, and H.-J. Güntherodt, Velocity dependence of atomic friction, *Phys. Rev. Lett.* **84**, 1172 (2000).
- [10] D. Dietzel, C. Ritter, T. Mönninghoff, H. Fuchs, A. Schirmeisen, and U. D. Schwarz, Frictional duality observed during nanoparticle sliding, *Phys. Rev. Lett.* **101**, 125505 (2008).
- [11] Y. Song, D. Mandelli, O. Hod, M. Urbakh, M. Ma, and Q. Zheng, Robust microscale superlubricity in graphite/hexagonal boron nitride layered heterojunctions, *Nat. Mater.* **17**, 894 (2018).

- [12] J. Krim, D. H. Solina, and R. Chiarello, Nanotribology of a Kr monolayer: A quartz-crystal microbalance study of atomic-scale friction, *Phys. Rev. Lett.* **66**, 181 (1991).
- [13] L. Prandtl, Ein Gedankenmodell Zur Kinetischen Theorie Der Festen Körper, *J. Appl. Math. Mech.* **8**, 85 (1928).
- [14] G. A. Tomlinson, A molecular theory of friction, *London, Edinburgh Philos. Mag. J. Sci.* **7**, 905 (1929).
- [15] T. Kontorova and J. Frenkel, On the theory of plastic deformation and twinning. II., *Zh. Eksp. Teor. Fiz.* **8**, 1340 (1938).
- [16] M. Weiss and F.-J. Elmer, Dry friction in the Frenkel-Kontorova-Tomlinson model: Static properties, *Phys. Rev. B* **53**, 7539 (1996).
- [17] M. Weiss and F.-J. Elmer, Dry friction in the Frenkel-Kontorova-Tomlinson model: Dynamical properties, *Z. Phys. B Condens. Matter* **104**, 55 (1997).
- [18] H. Hölscher, U. D. Schwarz, and R. Wiesendanger, Modelling of the scan process in lateral force microscopy, *Surf. Sci.* **375**, 395 (1997).
- [19] E. Riedo, E. Gneco, R. Bennewitz, E. Meyer, and H. Brune, Interaction potential and hopping dynamics governing sliding friction, *Phys. Rev. Lett.* **91**, 084502 (2003).
- [20] A. Schirmeisen, L. Jansen, H. Hölscher, and H. Fuchs, Temperature dependence of point contact friction on silicon, *Appl. Phys. Lett.* **88**, 123108 (2006).
- [21] Y. Sang, M. Dubé, and M. Grant, Thermal effects on atomic friction, *Phys. Rev. Lett.* **87**, 174301 (2001).
- [22] L. Jansen, H. Hölscher, H. Fuchs, and A. Schirmeisen, Temperature dependence of atomic-scale stick-slip friction, *Phys. Rev. Lett.* **104**, 256101 (2010).
- [23] S. Yu. Krylov, K. B. Jinesh, H. Valk, M. Dienwiebel, and J. W. M. Frenken, Thermally induced suppression of friction at the atomic scale, *Phys. Rev. E* **71**, 065101(R) (2005).
- [24] D. Gangloff, A. Bylinskii, I. Counts, W. Jhe, and V. Vuletić, Velocity tuning of friction with two trapped atoms, *Nat. Phys.* **11**, 915 (2015).
- [25] I. Barel, M. Urbakh, L. Jansen, and A. Schirmeisen, Unexpected temperature and velocity dependencies of atomic-scale stick-slip friction, *Phys. Rev. B* **84**, 115417 (2011).
- [26] E. A. Jagla, Velocity weakening and possibility of after-shocks in nanoscale friction experiments, *Phys. Rev. B* **86**, 155408 (2012).
- [27] Z. Duan, Z. Wei, S. Huang, Y. Wang, C. Sun, Y. Tao, Y. Dong, J. Yang, Y. Zhang, Y. Kan, D. Li, and Y. Chen, Resonance in atomic-scale sliding friction, *Nano Lett.* **21**, 4615 (2021).
- [28] See Supplemental Material at <http://link.aps.org/supplemental/10.1103/PhysRevLett.132.056203> for Sec. 1: MD simulation results, which includes Refs. [29–31]; Sec. 2: damping term derivation; Secs. 3–8: experimental details, which includes Refs. [32–34]; Secs. 9–15: more details of the phononic model.
- [29] L. Lindsay and D. A. Broido, Optimized Tersoff and Brenner empirical potential parameters for lattice dynamics and phonon thermal transport in carbon nanotubes and graphene, *Phys. Rev. B* **81**, 205441 (2010).
- [30] I. V. Lebedeva, A. A. Knizhnik, A. M. Popov, O. V. Ershova, Y. E. Lozovik, and B. V. Potapkin, Fast diffusion of a graphene flake on a graphene layer, *Phys. Rev. B* **82**, 155460 (2010).
- [31] Z. Wei, L. Xiang, Y. Kan, Y. Zhang, and Y. Chen, Effects of the normal load on the excited phonons in atomic friction, *J. Appl. Phys.* **132**, 175301 (2022).
- [32] J. L. Hutter and J. Bechhoefer, Calibration of atomic-force microscope tips, *Rev. Sci. Instrum.* **64**, 1868 (1993).
- [33] J. E. Sader, J. W. M. Chon, and P. Mulvaney, Calibration of rectangular atomic force microscope cantilevers, *Rev. Sci. Instrum.* **70**, 3967 (1999).
- [34] K. Wagner, P. Cheng, and D. Vezenov, Noncontact method for calibration of lateral forces in scanning force microscopy, *Langmuir* **27**, 4635 (2011).
- [35] M. H. Müser, Velocity dependence of kinetic friction in the Prandtl-Tomlinson model, *Phys. Rev. B* **84**, 125419 (2011).
- [36] Y. Dong, A. Vadakkepatt, and A. Martini, Analytical models for atomic friction, *Tribol. Lett.* **44**, 367 (2011).
- [37] S. A. Adelman, Generalized Langevin equation approach for atom/solid-surface scattering: General formulation for classical scattering off harmonic solids, *J. Chem. Phys.* **64**, 2375 (1976).
- [38] B. Fu and R. M. Espinosa-Marzal, Velocity-weakening and -strengthening friction at single and multiasperity contacts with calcite single crystals, *Proc. Natl. Acad. Sci. U.S.A.* **119**, e2112505119 (2022).
- [39] X. Banquy, D. D. Lowrey, N. Belman, Y. Min, G. Mordukhovich, and J. N. Israelachvili, Measurement and characterization of “resonance friction” at high sliding speeds in a model automotive wet clutch, *Tribol. Lett.* **43**, 185 (2011).
- [40] M. Evstigneev and P. Reimann, Thermally activated contact strengthening explains nonmonotonic temperature and velocity dependence of atomic friction, *Phys. Rev. X* **3**, 041020 (2013).
- [41] E. Granato and S. C. Ying, Non-monotonic velocity dependence of atomic friction, *Tribol. Lett.* **39**, 229 (2010).
- [42] J. Chen, I. Ratera, J. Y. Park, and M. Salmeron, Velocity dependence of friction and hydrogen bonding effects, *Phys. Rev. Lett.* **96**, 236102 (2006).
- [43] C. Fusco and A. Fasolino, Velocity dependence of atomic-scale friction: A comparative study of the one- and two-dimensional tomlinson model, *Phys. Rev. B* **71**, 045413 (2005).
- [44] M. Igarashi, J. Nakamura, and A. Natori, Mechanism of velocity saturation of atomic friction force and dynamic superlubricity at torsional resonance, *Jpn. J. Appl. Phys.* **46**, 5591 (2007).
- [45] K. L. Johnson and J. Woodhouse, Stick-slip motion in the atomic force microscope, *Tribol. Lett.* **5**, 155 (1998).
- [46] Y. Hoshi, T. Kawagishi, and H. Kawakatsu, Velocity dependence and limitations of friction force microscopy of mica and graphite, *Jpn. J. Appl. Phys.* **39**, 3804 (2000).
- [47] J. Klein, Frictional dissipation in stick-slip sliding, *Phys. Rev. Lett.* **98**, 056101 (2007).
- [48] S. Maier, Y. Sang, T. Filleter, M. Grant, R. Bennewitz, E. Gneco, and E. Meyer, Fluctuations and jump dynamics in atomic friction experiments, *Phys. Rev. B* **72**, 245418 (2005).